Ab initio effective interactions for *sd*-shell valence nucleons

E. Dikmen,[1,2,*] A. F. Lisetskiy,[2,†] B. R. Barrett,[2,‡] P. Maris,[3,§] A. M. Shirokov,[3,4,5,‖] and J. P. Vary[3,¶]

[1]*Department of Physics, Suleyman Demirel University, Isparta, Turkey*

[2]*Department of Physics, University of Arizona, Tucson, Arizona 85721, USA*

[3]*Department of Physics and Astronomy, Iowa State University, Ames, Iowa 50011, USA*

[4]*Skobeltsyn Institute of Nuclear Physics, Lomonosov Moscow State University, Moscow 119991, Russia*

[5]*Pacific National University, 136 Tikhookeanskaya st., Khabarovsk 680035, Russia*

(Received 7 February 2015; published 2 June 2015)

We perform *ab initio* no-core shell-model calculations for $A = 18$ and 19 nuclei in a $4\hbar\Omega$, or $N_{\max} = 4$, model space by using the effective JISP16 and chiral N3LO nucleon-nucleon potentials and transform the many-body effective Hamiltonians into the $0\hbar\Omega$ model space to construct the A-body effective Hamiltonians in the *sd* shell. We separate the A-body effective Hamiltonians with $A = 18$ and $A = 19$ into inert core, one-, and two-body components. Then we use these core, one-, and two-body components to perform standard shell-model calculations for the $A = 18$ and $A = 19$ systems with valence nucleons restricted to the *sd* shell. Finally, we compare the standard shell-model results in the $0\hbar\Omega$ model space with the exact no-core shell-model results in the $4\hbar\Omega$ model space for the $A = 18$ and $A = 19$ systems and find good agreement.

DOI: 10.1103/PhysRevC.91.064301 PACS number(s): 21.60.De, 21.60.Cs, 21.30.Fe, 27.20.+n

I. INTRODUCTION

In recent years remarkable progress in *ab initio* microscopic nuclear structure studies has been made in calculating nuclear properties, e.g., low-lying spectra, transition strengths, etc., in light nuclei. Large-basis *ab initio* no-core shell-model (NCSM) calculations, which provide the foundation for this investigation, have been successful in reproducing the low-lying spectra and other properties of nuclei with $A \leqslant 16$ [1–19].

In NCSM calculations all nucleons in the nucleus are active and are treated equivalently in the chosen model space. When we increase the model space to obtain more precise results, we encounter the problem that the size of the calculations can easily exceed currently available computational resources. This is especially true as one proceeds towards the upper end of *p*-shell nuclei and beyond. The problem may be cast as a challenge to reproduce the many-body correlations present in the large space in a tractable, smaller model space. Success in this endeavor will open up the prospects for *ab initio* solutions for a wider range of nuclei than are currently accessible.

The NCSM has proven to be an *ab initio* microscopic nuclear structure approach that has been able to reproduce experimental results and to make reliable predictions for nuclei with $A \leqslant 16$. These successes motivate us to develop approaches for heavier-mass nuclei. In one approach, a small model space effective interaction has been constructed by modifying the one-body piece of the effective two-body Hamiltonian and employing a unitary transformation in order to account for many-body correlations for the A-body system in a large space [20]. In another approach [21], the effective two- and three-body Hamiltonians for *p*-shell nuclei have been constructed by performing $12\hbar\Omega$ *ab initio* [i.e., $N_{\max} = 12$ harmonic oscillator (HO) quanta above the minimum required] NCSM calculations for $A = 6$ and $A = 7$ systems and explicitly projecting the many-body Hamiltonians onto the $0\hbar\Omega$ space. These A-dependent effective Hamiltonians can be separated into core, one-body, and two-body (and three-body) components, all of which are also A-dependent [21].

Recently, two more *ab initio* methods for valence nucleon effective interactions have been introduced with the same goals; one is based on the in-medium similarity renormalization group approach [22] and the other is based on the coupled-cluster method [23].

In this work, following the original idea of Refs. [11,21], we derive two-body effective interactions for the *sd* shell by using $4\hbar\Omega$ NCSM wave functions at the two-body cluster level, which contain all the many-body correlations of the $4\hbar\Omega$ no-core model space. The goal of this work is to demonstrate feasibility of this approach in the *sd* shell, where we do not require calculations at the limit of currently accessible computers. Such a major extension will be addressed in a future effort.

At the first step, we construct a "primary" effective Hamiltonian following the Okubo–Lee–Suzuki (OLS) unitary transformation method [24–26]. We indicate this first step schematically by the progression shown with the two large squares in the lower section of Fig. 1. We elect to perform this first step at the two-body-cluster level for ^{18}F in the $4\hbar\Omega$ model space (the "P-space") following the NCSM prescription [12,13,16]. For our initial interactions we select the JISP16 [27] and chiral N3LO [28] potentials. Our formalism may be directly adapted to include the three-nucleon force (3NF) but the computational effort increases dramatically. Thus, we do not include the 3NF in this initial work.

For the second step, we begin by performing a NCSM calculation for ^{18}F with the primary effective Hamiltonian in the $4\hbar\Omega$ model space to generate the low-lying eigenvalues

*erdaldikmen@sdu.edu.tr

†Present address: Mintec, Inc., Tucson, Arizona, USA; lisetsky@comcast.net

‡bbarrett@physics.arizona.edu

§pmaris@iastate.edu

‖shirokov@nucl-th.sinp.msu.ru

¶jvary@iastate.edu

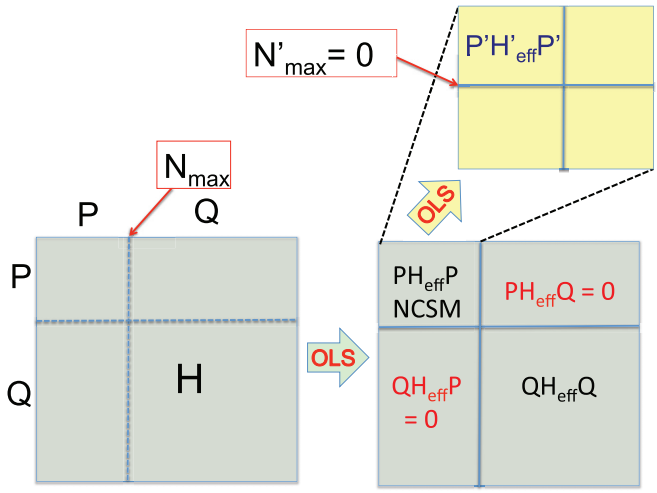

FIG. 1. (Color online) Flow of renormalizations adopted to derive an effective interaction for valence nucleons. The OLS procedure is first applied to derive a NCSM effective interaction for the full A-nucleon system resulting in the "primary" effective Hamiltonian $PH_{\rm eff}P$ for the chosen no-core basis space (the "P-space") indicated on the large square on the right of the figure in its upper-left corner. The many-body truncation is indicated by $N_{\rm max}$, the total number of HO quanta above the minimum for that system. The OLS procedure is applied again by using the results of the NCSM calculation to derive the "secondary" effective Hamiltonian $P'H'_{\rm eff}P'$ for the chosen valence space (the P'-space with the smaller many-body cutoff $N'_{\rm max}$) indicated on the square in the upper right of the figure.

and eigenvectors needed for a second OLS transformation, as indicated by the flow to the upper right in Fig. 1. These ^{18}F eigenvectors are dominated by configurations with an ^{16}O system in the lowest available HO orbits and two nucleons in the sd shell. All additional many-body correlations are also present. With these ^{18}F eigenvectors and eigenvalues we then solve for the "secondary" effective Hamiltonian, again using an OLS transformation, that acts only in the $N'_{\rm max} = 0$ space of ^{18}F but produces the same low-lying eigenvalues. Here we are following the scheme initially introduced in Ref. [11]. The matrix elements of this secondary effective Hamiltonian have the property that all configurations are defined with two nucleons in the sd space and an ^{16}O subsystem restricted to the lowest available HO single-particle states. This second step therefore produces a secondary effective Hamiltonian that is equivalent to what we would call the 18-body cluster Hamiltonian in the NCSM acting in the $N'_{\rm max} = 0$ space.

At the third step, we carry out NCSM calculations for the ^{16}O, ^{17}O, and ^{17}F systems with the primary effective interaction in the $4\hbar\Omega$ basis space. The results of these calculations produce, respectively, the core and one-body components included in the secondary effective Hamiltonian.

At the fourth step, we subtract the core and one-body terms from the secondary effective Hamiltonians of step 2 to obtain the effective valence interaction two–body matrix elements (TBMEs) in the sd-shell space.

Following the completion of these four steps, we then use the effective valence interaction matrix elements along with the extracted single-particle energies (for both the proton and the neutron) for standard shell-model (SSM) calculations in the sd-shell space.

For any system with $A > 18$, we can obtain its 18-body cluster Hamiltonian by repeating the entire procedure utilizing the primary effective Hamiltonian for that value of A. The second and subsequent steps remain the same. That is, we perform NCSM calculations with the primary (A-dependent) effective NN potential for ^{16}O, ^{17}O, ^{17}F, and ^{18}F in order to obtain the (A-dependent) core energy, single-particle energies, and TBMEs, which can then be used in a SSM calculation for that value of A. We provide details for applications to $A > 18$ systems below using ^{19}F as an example.

We employ the Coulomb interaction between the protons in the NCSM calculations which gives rise to the major shift between the derived neutron and proton single-particle energies. Exploration of full charge-dependence in the derived two-body valence interactions will be addressed in a future effort. In particular, our current $A = 18$ and 19 applications will have at most one valence proton so we do not require a residual Coulomb interaction between valence protons in this work.

For the chiral N3LO we retain full charge dependence in the first step—that is, when deriving the primary effective Hamiltonian. Thus, the A-body, core, and valence system calculations are performed with full charge dependence retained. Since we currently solve only for ^{18}F in step 2, we derive only the isospin-dependent but charge-independent secondary effective Hamiltonian. To retain full charge dependence in the secondary effective Hamiltonian, which would constitute predictions beyond conventional phenomenological interactions, would require additional ^{18}O and ^{18}Ne calculations that are intended in future efforts.

One may straightforwardly generalize these steps outlined above to solve for effective three-body valence interactions suitable for SSM calculations. Earlier efforts using an alternative implementation of step 3 [21] showed that effective three-body valence interactions lead to significant improvements over effective two-body valence interactions.

II. THEORETICAL DESCRIPTION

A. No-core shell model and effective interaction

The NCSM calculations start with the intrinsic Hamiltonian of the A-nucleon system, omitting any 3NF in the present effort:

$$H = \sum_{i<j=1}^{A} \frac{(\vec{p}_i - \vec{p}_j)^2}{2Am} + \sum_{i<j=1}^{A} V_{ij}^{NN} = T_{\rm rel} + V^{NN}, \quad (1)$$

where m is the nucleon mass, V_{ij}^{NN} is the bare NN interaction, $T_{\rm rel}$ is the relative kinetic energy and V^{NN} is the total two-body interaction. We will add the Coulomb interaction between the protons at a later stage since we treat it as a perturbative correction to the derived primary effective Hamiltonian. In order to facilitate convergence, we modify Eq. (1) by adding (and later subtracting) the center-of-mass HO Hamiltonian which introduces a dependence on the HO energy, $\hbar\Omega$, and this

dependence is denoted by "Ω" in what follows. In addition, we introduce $a \leqslant A$ to define a new a-, A-, and Ω-dependent Hamiltonian:

$$H_a = \sum_{i=1}^{a}\left[\frac{\vec{p}_i{}^2}{2m} + \frac{1}{2}m\Omega^2\vec{r}_i{}^2\right] + \sum_{i<j=1}^{a} V_{ij}(\Omega, A), \quad (2)$$

where $a = A$ corresponds to the full Hamiltonian of Eq. (1) with the center-of-mass HO Hamiltonian added and $V_{ij}(\Omega, A)$ is the modified bare NN interaction which we define independent of the parameter a but including dependence on A:

$$V_{ij}(\Omega, A) = V_{ij}^{NN} - \frac{m\Omega^2}{2A}(\vec{r}_i - \vec{r}_j)^2. \quad (3)$$

The exact solution of Eq. (1) for a subset of its eigensolutions in a finite matrix diagonalization requires the derivation of an A-body effective interaction for sufficiently heavy nuclei [16], but such a derivation is not currently possible for $A > 5$ with realistic interactions.

Here, we adopt the two-body cluster approximation ($a = 2$) for the effective interaction [12,13]. This allows us to solve the eigenvalue problem for a sufficiently large basis space that we achieve convergence of a suitable set of low-lying eigenvalues and eigenvectors needed to construct the primary effective Hamiltonian. In the $a = 2$ approximation, the Hamiltonian (2) becomes

$$H_2 = \sum_{i=1}^{2}\left[\frac{\vec{p}_i{}^2}{2m} + \frac{1}{2}m\Omega^2\vec{r}_i{}^2\right] + V_{12}(\Omega, A). \quad (4)$$

For deriving an effective three-nucleon interaction one would take $a = 3$. Note that the A dependence enters the Hamiltonian H_2 through the second term in Eq. (3). For example, this A dependence makes the two-body cluster Hamiltonian H_2 in the $T = 0$ channel different from the deuteron Hamiltonian. In order to preserve Galilean invariance in the primary effective Hamiltonian, we obtain the solutions to Eq. (4) in the relative HO basis where the the center-of-mass component of the first term in Eq. (4) plays no role.

We now introduce our representation of the unitary transformation needed to construct the primary effective Hamiltonian $PH_{\rm eff}P := H_2^P$ in the P space (signified by a superscript "P") of the first step. The P-space effective interactions have A dependence, Ω dependence and $N_{\rm max}$ dependence all implied by the superscript P. We define $N_{\rm max}$ as the maximum number of HO quanta in the many-body HO basis space (the NCSM basis space) above the minimum for the A-nucleon nucleus. We select $N_{\rm max} = 4$ in the present work. The resulting finite P space, of dimension d_P, for the first step is indicated on the left-hand side of Fig. 1. The diagonalization of the Hamiltonian H_2 in the relative HO basis provides the unitary transformation U_2 such that

$$H_{2;\rm diag} = U_2 H_2 U_2^\dagger, \quad (5)$$

where $H_{2;\rm diag}$ is the diagonal matrix containing the eigenvalues $E_{2;k}$:

$$H_{2;\rm diag} = \begin{pmatrix} E_{2;1} & 0 & \cdots & 0 \\ 0 & E_{2;2} & \cdots & 0 \\ \cdots & \cdots & \cdots & \cdots \\ 0 & 0 & 0 & E_{2;\rm max} \end{pmatrix}, \quad (6)$$

where the subscript "max" signifies the dimension of the $a = 2$ space sufficient to guarantee convergence of the d_P low-lying eigenvalues and eigenvectors. We typically employ max = 200 to 450 for a realistic NN interaction governed by the need to converge the results for the chosen interaction at the selected value of $\hbar\Omega$.

By introducing the model space P, one builds the matrix $H_{2;\rm diag}^P = PH_{2;\rm diag}P$:

$$H_{2;\rm diag}^P = \begin{pmatrix} E_{2;1} & 0 & \cdots & 0 \\ 0 & E_{2;2} & \cdots & 0 \\ \cdots & \cdots & \cdots & \cdots \\ 0 & 0 & 0 & E_{2;d_P} \end{pmatrix}. \quad (7)$$

The unitary transformation matrix U_a in which $a = 2$ refers to two-body cluster approximation and can be split into four blocks corresponding to the blocks within the large squares of Fig. 1:

$$U_a = \begin{pmatrix} U_a^P & U_a^{PQ} \\ U_a^{QP} & U_a^Q \end{pmatrix}, \quad (8)$$

where the matrix U_a^P is the $d_P \times d_P$ square matrix corresponding to the P space. One constructs the U_2^P matrix from the U_a matrix by taking d_P rows and columns of the eigenvectors corresponding to the chosen d_P eigenvalues:

$$U_2^P = \begin{pmatrix} b_{1,1} & b_{1,2} & \cdots & b_{1,d_P} \\ b_{2,1} & b_{2,2} & \cdots & b_{2,d_P} \\ \cdots & \cdots & \cdots & \cdots \\ b_{d_P,1} & b_{d_P,2} & \cdots & b_{d_P,d_P} \end{pmatrix}. \quad (9)$$

The primary effective Hamiltonian H_2^P, signified by the box labeled "$PH_{\rm eff}P$" in Fig. 1, can then be calculated by using the following formula:

$$H_2^P = \frac{U_2^{P\dagger}}{\sqrt{U_2^{P\dagger}U_2^P}} H_{2;\rm diag}^P \frac{U_2^P}{\sqrt{U_2^{P\dagger}U_2^P}} = T_{\rm rel} + V_{\rm eff}^P, \quad (10)$$

where $V_{\rm eff}^P$ is the resulting primary effective NN interaction and we suppress the subscript "2." The interaction $V_{\rm eff}^P$ depends on A and the chosen P space including the selected value of Ω. Note that the unitary transformation (10) is identical to OLS unitary transformation [24–26] which satisfies the decoupling condition $QH_{\rm eff}P := H_2^{QP} = 0$ where the submatrix $QH_{\rm eff}P = 0$ is one of two decoupling conditions depicted in Fig. 1 for the primary Hamiltonian.

There are certain freedoms within the OLS renormalization procedure as well as mathematical restrictions [29]. In this context, we note that in, our application, we select the d_P

lowest eigenvalues and eigenvectors of H_2 for input to our primary effective Hamiltonian through Eq. (7) and obtain numerically stable and accurate results.

B. Transformation of many-body Hamiltonian into *sd*-shell space

After a unitary transformation of the bare Hamiltonian in Eq. (4) to the $4\hbar\Omega$ ($N_{\max}=4$) model space for the case of ^{18}F, we calculate the 18-body effective Hamiltonian $PH_{\rm eff}P := H_{18}^{P}$ in the $4\hbar\Omega$ space and solve for its low-lying eigenvalues and eigenvectors in a NCSM calculation. This is analogous to solving the $a=2$ case above so we introduce the corresponding subscript 18. We obtain a sufficient number of these 18-body solutions to generate a second unitary transformation to take H_{18}^{P} from the $4\hbar\Omega$ model space to a smaller secondary subspace P', e.g., the *sd*-shell space, given by $N'_{\max}=0$. The secondary effective Hamiltonian is called $H_{a'}^{P'P}$ with $a'=18$ and is represented by $P'H'_{\rm eff}P'$ in Fig. 1.

This "second step" outlined above follows a similar path to the "first step" and is indicated by the work flow at the upper right in Fig. 1. Note that the P space in the first unitary transformation is now split into parts related to the two subspaces, P' and Q', where $P'+Q'=P$. Our secondary effective Hamiltonian $H_{18}^{P'P}$ is designed to reproduce exactly the lowest $d_{P'}$ eigenvalues of the primary effective Hamiltonian H_{18}^{P} through

$$H_{18}^{P'P} = \frac{U_{18}^{P'\dagger}}{\sqrt{U_{18}^{P'\dagger}U_{18}^{P'}}} H_{18;\rm diag}^{P'} \frac{U_{18}^{P'}}{\sqrt{U_{18}^{P'\dagger}U_{18}^{P'}}} = T_{\rm rel} + V_{\rm eff}^{P'P}, \tag{11}$$

where $V_{\rm eff}^{P'P}$ is the resulting secondary effective interaction and we suppress the label for the $a'=18$ dependence.

This secondary effective Hamiltonian (11) is, in general, an 18-body operator. However, in the $N'_{\max}=0$ case, the matrix dimension of the 18-body secondary effective Hamiltonian (11) is the same as the matrix dimension of a one-body plus two-body effective Hamiltonian acting in the *sd*-shell space. This means that $H_{18}^{P'P}$ can be taken to consist of only one-body and two-body terms, even after the exact 18-body cluster transformation. All the orbitals below the *sd*-shell space are fully occupied by the other 16 nucleon spectators, and the total 18-body wave function can be exactly factorized into a 16-body 0^+ and two-body *sd*-shell wave functions. This considerably simplifies calculations with $H_{18}^{P'P}$. Therefore, we can write a' as $a'=a_{\rm c}+a_{\rm v}$, where $a_{\rm c}$ is the number of core nucleons (16 in this case) and $a_{\rm v}$ is the size of the valence cluster.

In the third step outlined above we solve for the eigenvalues of ^{17}F and ^{17}O in the P space by using the effective interaction $V_{\rm eff}^{P}$ from Eq. (10) joined with the $T_{\rm rel}$ for $A=17$ to obtain the proton and neutron one-body terms of the secondary effective Hamiltonian in the *sd*-shell space. Then we subtract the one-body terms from the secondary effective Hamiltonian of ^{18}F, and we obtain the effective "residual two-body interaction" matrix elements (or simply the TBMEs) in the *sd*-shell space. Additionally, in the third step, we evaluate the ^{16}O core energy by solving for its ground-state energy using the effective interaction $V_{\rm eff}^{P}$ from Eq. (10) joined with $T_{\rm rel}$ for ^{16}O.

Here, we adopt the $A=16$ (17) relative-kinetic-energy operators for NCSM evaluations of the core (single-particle) energies in step three. In earlier papers [21,30], based on the NCSM with a core first developed in Ref. [11], a much stronger A dependence was obtained than in our present *sd*-shell calculations. We now understand these earlier results in terms of how the core and single-particle energies are calculated. In these earlier studies, the A dependence of the kinetic-energy operator in the many-nucleon Hamiltonian used for calculating the core and single-particle energies was taken to be the total A of the nucleus being studied. In our current calculations, we use $A(\text{core})=16$ for the kinetic-energy operator when calculating the core energy and $A(\text{core}+1)=17$ when calculating the single-particle energies, independent of the total A of the nucleus being studied. Because the A dependence of the kinetic-energy operator goes as $1/A$, using the total A instead of $A(\text{core})$ or $A(\text{core}+1)$ produces a much larger A dependence of the core and single-particle energies. Both these choices are technically correct (i.e., they produce identical results for the nucleus being studied, as we have verified) and merely reflect that these effective valence-space interactions are not uniquely defined. With our current choice, we achieve weak A dependence of our resulting core, single-particle, and valence effective interactions for *sd*-shell applications, which is appealing since this is a characteristic that is commonly found in phenomenological effective interactions. Our weak A dependence is also consistent with other *ab initio* investigations using either the IM-SRG technique [22] or the coupled-cluster method [23].

We then proceed to the fourth step and subtract this core energy from the energies of the single-particle states of ^{17}F and ^{17}O mentioned above to arrive at our valence single-particle energies. At the completion of step four, we have our twobody valence-core (2BVC) effective Hamiltonian that may be used in standard shell-model (SSM) calculations.

By using these core plus valence space single-particle energies along with the derived residual two-body effective interactions, we can perform the SSM calculations for ^{18}F, as well as other nuclei, in the *sd* shell and compare with full NCSM calculations in the $4\hbar\Omega$ space by using the primary effective Hamiltonian. The SSM calculations for ^{18}F will, by construction, give the same results as the NCSM calculations for ^{18}F within numerical precision. A corresponding approach for $A>18$ nuclei is exemplified below where we also provide a direct comparison between NCSM and SSM results. One may then proceed, in principle, with SSM calculations to cases where full NCSM results are beyond current technical means.

We may summarize the results of steps 2–4 by arranging the results for the secondary effective Hamiltonian $H_{a'}^{P'P}$ into separate terms:

$$H_{a'}^{P'P} = H_{a_c}^{P'P} + H_{\rm sp}^{P'P} + V_{a_v}^{P'P}, \tag{12}$$

where we have allowed for the more general case of two successive renormalization steps (signified by $P'P$) with $a'=A$ in the present discussion. In Eq. (12) H_{a_c} represents the core Hamiltonian for a_c nucleons; $H_{\rm sp}$ represents the valence nucleon single-particle Hamiltonian and V_{a_v} represents the

a_v-body residual effective valence interaction. Note that V_{a_v} may be used for systems with more than a_v valence nucleons, as we demonstrate below. We also note that the core and the valence single-particle Hamiltonians include their respective kinetic-energy terms.

In line with our approximations mentioned above, we use ^{18}F alone to derive our isospin-dependent effective two-body interaction $V_2^{P'P}$ for the *sd* shell. We then restrict our applications, at present, to cases with at most one proton in the *sd* shell.

In SSM calculations, one typically uses only the $H_{\rm sp}$ and V_{a_v} terms in Eq. (12). In phenomenological Hamiltonians $H_{\rm sp}$ is often taken from experiment and $a_v = 2$ matrix elements are obtained by fits to properties of a set of nuclei. We will present detailed comparisons between our derived $H_{\rm sp}$ and V_{a_v} terms with phenomenological interactions in a future presentation.

There is an important distinction between our SSM calculations (with our Hamiltonian derived from the *ab initio* NCSM) and conventional SSM calculations with phenomenological interactions. We preserve the factorization of the CM motion throughout our derivation for the primary and secondary effective Hamiltonians. Therefore, the $N'_{\rm max} = 0$ secondary effective Hamiltonian not only reproduces the appropriate $N_{\rm max}$ NCSM eigenvalues but also affords access to wave functions for these $N'_{\rm max} = 0$ states which may be written with a factorized CM wave function of the entire system.

III. EFFECTIVE TWO-BODY *sd*-SHELL INTERACTION

In NCSM calculations, the dimension of the primary effective Hamiltonian increases very rapidly as we increase $N_{\rm max}$ and/or the number of nucleons. We restricted the model space to $N_{\rm max} = 4$ in order to limit the computational effort, since our main goal is to demonstrate the procedure to obtain effective interactions in the *sd* shell for the shell model with the ^{16}O core using the *ab initio* NCSM and to test these derived effective interactions with SSM calculations. In order to carry out NCSM calculations, we used the MFDn code [31–33] with the JISP16 and chiral N3LO NN interactions. For the SSM calculations, we used a specialized version of the shell-model code ANTOINE [34–36].

A. Core and valence effective interactions for $A = 18$ system

Following the methods presented in Sec. II for H_2^P in Eq. (10), we calculated the 18-body primary effective Hamiltonians with $N_{\rm max} = 4$ and $\hbar\Omega = 14$ MeV by using the bare JISP16 [27] and chiral N3LO [28] potentials for V_{ij}^{NN}. We chose $\hbar\Omega = 14$ MeV since it is near the minimum of the ground-state energy of ^{16}O at $N_{\rm max} = 4$ [27] and it represents a typical choice for derived effective shell-model valence interactions (see, for example, Ref. [37]). Future efforts with primary effective Hamiltonians derived in larger-$N_{\rm max}$ spaces will be needed for meaningful analyses of the $\hbar\Omega$ dependence of our results.

We solve for the ^{18}F spectra in NCSM calculations with these primary effective Hamiltonians and present the lowest 28 eigenvalues in Table I. The corresponding NCSM eigenvectors for these 28 states in the $N_{\rm max} = 4$ space are the eigenvectors dominated by $N_{\rm max} = 0$ components. These 28 eigenstates correspond with the complete set of $N_{\rm max} = 0$ states in the *sd* shell.

TABLE I. The NCSM energies (in MeV) of the lowest 28 states J_i^π of ^{18}F calculated in $4\hbar\Omega$ model space by using JISP16 and chiral N3LO NN interactions with $\hbar\Omega = 14$ MeV.

J_i^π	T	JISP16	J_i^π	T	N3LO
1_1^+	0	−122.742	1_1^+	0	−126.964
3_1^+	0	−122.055	3_1^+	0	−126.214
0_1^+	1	−121.320	0_1^+	1	−125.510
5_1^+	0	−120.329	5_1^+	0	−124.545
2_1^+	1	−119.505	2_1^+	1	−123.974
2_2^+	0	−119.011	2_2^+	0	−123.890
1_2^+	0	−118.709	1_2^+	0	−123.077
0_2^+	1	−118.410	0_2^+	1	−122.586
2_3^+	1	−117.211	2_3^+	1	−121.588
3_2^+	1	−117.035	4_1^+	1	−121.512
4_1^+	1	−117.004	3_2^+	1	−121.450
3_3^+	0	−116.765	3_3^+	0	−121.376
1_3^+	0	−113.565	1_3^+	0	−119.658
4_2^+	0	−112.314	4_2^+	0	−118.656
2_4^+	0	−111.899	2_4^+	0	−117.950
1_4^+	0	−110.357	1_4^+	0	−116.106
4_3^+	1	−109.625	4_3^+	1	−115.785
2_5^+	1	−109.292	2_5^+	1	−115.407
1_5^+	1	−108.752	3_4^+	0	−115.309
3_4^+	0	−108.706	1_5^+	1	−114.870
2_6^+	0	−108.485	2_6^+	0	−114.787
1_6^+	1	−108.055	1_6^+	1	−114.392
2_7^+	1	−108.041	3_5^+	1	−114.258
3_5^+	1	−107.874	2_7^+	1	−114.176
3_6^+	0	−101.528	3_6^+	0	−109.316
1_7^+	0	−99.946	1_7^+	0	−107.798
0_3^+	1	−99.848	2_8^+	1	−107.473
2_8^+	1	−99.607	0_3^+	1	−107.436

For each of these primary effective Hamiltonians H_2^P we then followed steps 2–4 above to calculate secondary effective Hamiltonians $H_{18}^{P'P}$ as well as the resulting six valence single-particle energies $H_{\rm sp}^{P'P}$ (three for neutrons and three for protons) and 63 valence two-body effective interaction matrix elements of $V_2^{P'P}$ in the coupled JT representation.

We now elaborate on the method of separating the secondary effective Hamiltonian $H_{18}^{P'P}$ into its components indicated in Eq. (12). According to step 3 we first perform separate NCSM calculations for ^{17}F and ^{17}O using the Hamiltonian consisting of the same $V_{\rm eff}^P$ from Eq. (10) combined with $T_{\rm rel}$ for $A = 17$. These two calculations provide total single-particle energies for the valence protons and neutrons, respectively, that are expressed as matrix elements of $H_{a_c}^{P'P} + H_{\rm sp}^{P'P}$.

We continue with the second part of step 3 to obtain the core energy ($E_{\rm core}$) through a NCSM calculation for ^{16}O by using the Hamiltonian consisting of $V_{\rm eff}^P$ from Eq. (10) in

combination with $T_{\rm rel}$ for ^{16}O. The resulting ^{16}O ground-state energy defines the contribution of $H_{a_c}^{P'P}$ to the matrix elements of $H_{a_c}^{P'P} + H_{\rm sp}^{P'P}$ obtained in the ^{17}F and ^{17}O calculations. The valence single-particle energies, the eigenvalues of $H_{\rm sp}^{P'P}$, are then defined as the total single-particle energies less the core energy.

To obtain the TBMEs of the valence effective interaction $V_2^{P'P}$, we execute step 4 and subtract the contributions of the core and valence single-particle energies from the matrix elements of $H_{18}^{P'P}$ to isolate $V_2^{P'P}$ in Eq. (12). To be specific, we designate our valence single-particle states by their angular momenta $j_i = \frac{1}{2}, \frac{3}{2}, \frac{5}{2}$. Then, we define the contribution to the doubly reduced coupled-JT TBMEs (signified by the subscript JT on the TBME) arising from the core and one-body terms as

$$\langle j_a j_b || H_{a_c}^{P'P} + H_{\rm sp}^{P'P} || j_c j_d \rangle_{JT} = \left[E_{\rm core} + \tfrac{1}{2}\left(\epsilon_{j_a}^n + \epsilon_{j_a}^p + \epsilon_{j_b}^n + \epsilon_{j_b}^p\right)\right] \delta_{j_a,j_c}\delta_{j_b,j_d}, \quad (13)$$

where ϵ_j represents the valence single-particle energy for the orbital with angular momentum j and the superscript n (p), designates neutron (proton) for the energy associated with the ^{17}O (^{17}F) calculation, respectively.

The resulting doubly reduced coupled-JT TBMEs of the valence effective interaction $V_2^{P'P}$ are expressed as

$$\langle j_a j_b || V_2^{P'P} || j_c j_d \rangle_{JT} = \langle j_a j_b || H_{a'}^{P'P} - H_{a_c}^{P'P} - H_{\rm sp}^{P'P} || j_c j_d \rangle_{JT}. \quad (14)$$

By using the symmetries of the coupled-JT representation, there are 63 unique TBMEs for which $j_a \leqslant j_b$.

We confirm the accuracy of this subtraction procedure by demonstrating that SSM calculations with the derived core, one-body, and two-body terms of Eq. (12) in the sd-shell space reproduce the absolute energies of the lowest 28 states of the $4\hbar\Omega$ NCSM calculations for ^{18}F shown in Table I.

The results for the core energy ($E_{\rm core}$) and valence single-particle energies (ϵ_j^n,ϵ_j^p) for the JISP16 interaction are presented on the left-hand side of Table II for our leading example where the primary effective Hamiltonian is derived for $A = 18$. The corresponding core energy and valence single-particle energy results for the chiral N3LO interaction are presented on the left-hand side of Table III. The valence single-particle energies clearly reflect overall Coulomb energy shifts between NCSM calculations for ^{17}F and ^{17}O.

The resulting TBMEs of the secondary effective Hamiltonian $H_{18}^{P'P}$ in Eq. (11) and of the valence effective interaction

TABLE II. Proton and neutron single-particle energies (in MeV) for JISP16 effective interaction obtained for the mass of $A = 18$ and $A = 19$.

j_i	$A = 18$, $E_{\rm core} = -115.529$			$A = 19$, $E_{\rm core} = -115.319$		
	$\frac{1}{2}$	$\frac{5}{2}$	$\frac{3}{2}$	$\frac{1}{2}$	$\frac{5}{2}$	$\frac{3}{2}$
$\epsilon_{j_i}^n$	−3.068	−2.270	6.262	−3.044	−2.248	6.289
$\epsilon_{j_i}^p$	0.603	1.398	9.748	0.627	1.419	9.774

TABLE III. Proton and neutron single-particle energies (in MeV) for chiral N3LO effective interaction obtained for the mass of $A = 18$ and $A = 19$.

j_i	$A = 18$, $E_{\rm core} = -118.469$			$A = 19$, $E_{\rm core} = -118.306$		
	$\frac{1}{2}$	$\frac{5}{2}$	$\frac{3}{2}$	$\frac{1}{2}$	$\frac{5}{2}$	$\frac{3}{2}$
$\epsilon_{j_i}^n$	−3.638	−3.042	3.763	−3.625	−3.031	3.770
$\epsilon_{j_i}^p$	0.044	0.690	7.299	0.057	0.700	7.307

$V_2^{P'P}$ in Eq. (14) are given in the seventh and eighth columns respectively of Tables IV and V in the Appendix. The results of Table IV are obtained with the JISP16NN interaction while those in Table V are obtained with the chiral N3LO NN interaction.

These results for $A = 18$ with JISP16 presented in Tables II and IV (as well as the corresponding results with chiral N3LO in Tables III and V) show the dominant contribution of $E_{\rm core}$ to the diagonal TBMEs of the secondary effective Hamiltonian $H_{18}^{P'P}$, as may be expected. When these $E_{\rm core}$ contributions along with the one-body contributions subtracted following Eq. (14), the resulting diagonal matrix elements of $V_2^{P'P}$ fall in the range of conventional phenomenological valence nucleon effective interactions. The nondiagonal TBMEs for $A = 18$ shown in columns seven and eight of Tables IV and V remain unchanged by the subtraction process of Eq. (14) as required by the Kronecker deltas in Eq. (13).

The resulting TBMEs of $V_2^{P'P}$ in column eight of Tables IV and V (see tables in the Appendix) appear highly correlated, as shown in Fig. 2, indicating significant independence of the valence nucleon interactions from the underlying realistic NN interaction. On the other hand, there is a noticeable dependence on the NN interaction seen in the spin-orbit splitting of the valence single-particle energies in Tables II and III. For both the splitting of the $d_{5/2}$ and $d_{3/2}$ orbitals, and the splitting of the $s_{1/2}$ and the $d_{3/2}$ orbitals, the JISP16 interaction produces significantly larger results than the chiral N3LO interaction. This is most noticeable in the approximately 30%, or 2 MeV, larger splittings of the $d_{5/2}$ and $d_{3/2}$ orbitals obtained with JISP16.

Note that both JISP16 and N3LO lead to splittings of the $d_{5/2}$ and $d_{3/2}$ orbitals that are larger than the phenomenological shell-model result which is based on experiment. In addition, the order of the calculated $s_{1/2}$ and $d_{5/2}$ orbitals are inverted compared with experiment. That is, ^{17}F and ^{17}O have a $5/2^+$ ground state, an excited $1/2^+$ at about 0.5 and 0.9 MeV respectively, and an excited $3/2^+$ at about 5 MeV. Of course, neither JISP16 nor the chiral N3LO interaction have been fit to any observable in the sd shell. In addition, these calculated splittings should be sensitive to the 3NF, which is known to impact spin-orbit coupling effects in p-shell NCSM investigations [8,15–17,19].

B. Two-body valence cluster approximation for $A = 19$ system

We now illustrate our approach for going to heavier nuclei by adopting the specific example of ^{19}F. In theory, we could

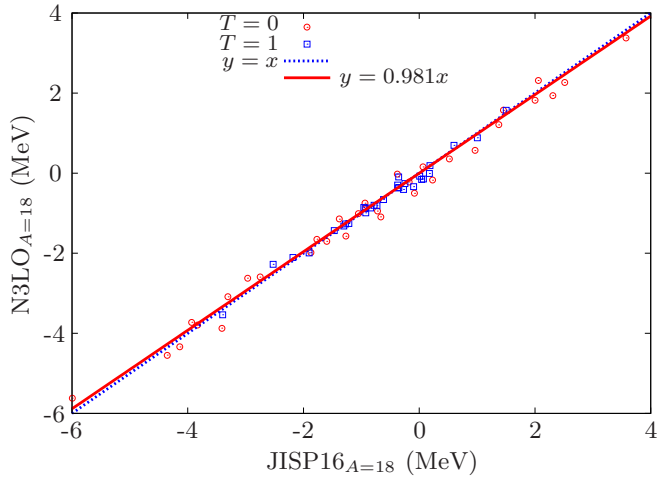

FIG. 2. (Color online) Correlation between chiral N3LO and JISP16 TBMEs plotted in units of MeV. The 63 TBMEs are derived for $A = 18$ with the methods described in the text and are presented in the eighth columns of Tables IV and V. Red circles (blue squares) represent $T = 0$ (1) matrix elements. The diagonal dashed line is the reference for equal matrix elements. The solid red line is a linear fit to the correlation points with the result $y = 0.981x$. The root-mean-square deviation between the two sets of TBMEs is 0.203 MeV. A plot of the $A = 19$ results in the tenth columns of Tables IV and V would be nearly indistinguishable from this plot.

proceed as with our application in the previous section; retain $a_c = 16$ and increase a_v in pace with the increase with A. Thus, for $A = 19$ we would derive matrix elements of an effective valence 3NF. However, this is not a practical path since there is no net gain over performing full NCSM calculations for each A *en route* to the secondary effective Hamiltonian. Instead, we present an alternative approximate path to heavier nuclei.

Our procedure for going to heavier nuclei in the sd shell is to specify the sd-shell nucleus of interest with its value of A in the first step—the construction of the primary effective interaction $V_{\rm eff}^P$ of Eq. (10). Then we define the two-body cluster Hamiltonian in Eq. (4) with this new value of A ($A = 19$ in our specific example) which is subsequently used to construct the primary effective interaction. Next, we perform steps 2–4 as before with $a_c = 16$, $a_v = 2$, and neglecting effective many-valence-nucleon interactions: we perform ^{18}F, ^{17}F, ^{17}O, and ^{16}O NCSM calculations with this primary effective interaction $V_{\rm eff}^P$ in order to extract the core energy, proton and neutron single-particle energies, and valence TBMEs. This is the 2BVC applied for general A. The generalization to $a_v = 3$ (the 3BVC approximation) is straightforward but computationally demanding. Note that for $A = 19$ the 3BVC would correspond to a complete NCSM calculation.

As an alternative, one may simply neglect any A dependence of the core energy, valence single-particle energies, and valence TBMEs and perform SSM calculations throughout the sd shell with the effective shell-model interaction derived for ^{18}F. We also illustrate this choice below with the example of ^{19}F.

We now investigate the consequences of neglecting the induced 3NF and of neglecting the A dependence of $V_{\rm eff}^P$. That is, we simply use the the derived core energy, valence single-particle energies, and valence TBMEs from the previous section in a SSM calculation of ^{19}F. For comparison, we also derive these quantities specifically for the ^{19}F system in the 2BVC approximation, and we compare both with a complete NCSM calculations for ^{19}F, which corresponds to performing the 3BVC approximation.

For the 2BVC approach to ^{19}F, we perform step 1 beginning with $A = 19$ instead of $A = 18$ in Eqs. (1)–(4). That is, we calculate the primary effective Hamiltonian of Eq. (10) for ^{19}F instead of ^{18}F. Then we proceed through the remaining equations, as we did for ^{18}F, using $V_{\rm eff}^P$ defined in Eq. (10). For example, in the second step we solve for the secondary effective Hamiltonian $H_{a'}^{P'P}$ with $a' = 18$ at $N_{\rm max} = 4$ using Eq. (11) as before. This establishes the foundation for proceeding with steps 3 and 4 to obtain the core energy, valence single-particle energies and valence TBMEs needed for solving ^{19}F in a SSM calculation.

The resulting core energies and valence single-particle energies calculated by using JISP16 and chiral N3LO effective interactions are given in the right-hand columns of Tables II and III, respectively. The core energies for the $A = 19$ case are less attractive than the $A = 18$ case by 210 keV (163 keV) for JISP16 (chiral N3LO). The single-particle energies for the $A = 18$ and $A = 19$ cases differ by less than 30 keV (20 keV) for JISP16 (chiral N3LO). We observe, therefore, that the core and single-particle energies exhibit similarly weak A dependence for both interactions.

The resulting TBMEs of the secondary effective Hamiltonian $H_{18}^{P'P}$ in Eq. (11) and of the valence effective interaction $V_2^{P'P}$ in Eq. (14) are given in the ninth and tenth columns, respectively, of Table IV (for JISP16) and Table V (for chiral N3LO) in the Appendix. One observes a good correlation between the TBME results from the $A = 18$ case and the $A = 19$ case by comparing column seven with column nine and column eight with column ten in both Tables IV (for JISP16) and V (for chiral N3LO). The TBME's of $V_2^{P'P}$ exhibit particularly weak A dependence. The largest difference between the TBMEs in columns eight and ten in Table IV (for JISP16) is 9 keV and the corresponding largest difference in Table V (for chiral N3LO) is 4 keV.

Our observed weak A dependence of the core energies, valence single-particle energies, and TBMEs is consistent with the view that the OLS transformation to the P space accounts for the high-momentum components of the NN interaction and the results are approximately independent of whether the two-body cluster is treated as embedded in $A = 18$ or in $A = 19$. The similarity of the derived TBMEs is also suggestive of a common, or universal, soft effective NN interaction.

We may elaborate on these points by noting that the first OLS transformation can be viewed as reducing the ultraviolet (UV) regulator of the JISP16 and N3LO interactions to the UV scale of the HO basis space limit controlled by $N_{\rm max}$ and by $\hbar\Omega$. The HO basis space UV regulator imposed by our first OLS transformation may be estimated by using N, the maximum of $2n + l$ of the HO single-particle orbits included in the P space. For ^{18}F (or ^{19}F) with $N_{\rm max} = 4$ and $\hbar\Omega = 14$ MeV

this UV regulator is estimated to be either $\sqrt{(N+3/2)m\Omega} = 1.59$ fm^{-1} according to Ref. [38] or $\sqrt{2(N+3/2+2)m\Omega} = 2.53$ fm^{-1} according to Ref. [39]. In either case, the estimated UV regulator is independent of A and is sufficiently low that we may speculate that our chosen NN interactions are yielding a common (or universal) UV-regulated primary effective NN interaction with the UV-regulation scale fixed by our choice of P space. Subsequent processing through the second OLS transformation is the same for both primary effective NN interactions so it retains that universality feature.

C. SSM and NCSM calculations for ^{18}F and ^{19}F with $A = 18$ and $A = 19$ interactions

We performed SSM calculations for the ground state and a few low-lying excited states of ^{18}F and ^{19}F by using the secondary effective Hamiltonians $H_{18}^{P'P}$ of Eq. (12) developed from the JISP16 and chiral N3LO potentials. We performed these SSM calculations with the code ANTOINE [34–36] by explicitly summing the one-body and two-body components on the right-hand side of Eq. (12) whose matrix elements are presented in Tables II and IV for JISP16 and in Tables III and V for chiral N3LO. Next, we add the respective core energy to the resulting spectra to yield total energies for comparison with NCSM calculations performed with the primary effective Hamiltonian.

We also carried out NCSM calculations for ^{18}F and ^{19}F by using the primary effective Hamiltonians H_2^P of Eq. (10) which are based on the selected NN interaction and on the selected A in Eqs. (1)–(4). The SSM and NCSM results for the ground state and a few low-lying excited states of ^{18}F and ^{19}F are shown in Fig. 3 for JISP16 and in Fig. 4 for chiral N3LO. The nucleus for which the spectra are presented (^{18}F or ^{19}F) is specified at the top of each column along with the many-body method—either NCSM with the primary effective Hamiltonian or SSM with the secondary effective Hamiltonian. Below each column we specify the A used in Eqs. (1)–(4). When the results of the NCSM and SSM are the same with both many-body methods (as they should be theoretically for ^{18}F), they appear as a single column with the label "NCSM/SSM." This situation, a simple cross-check of the manipulations and the codes, is presented in the first column of Fig. 3 for JISP16 and of Fig. 4 for chiral N3LO. Although these figures show only the lowest states, the cross-check is verified for all 28 states of two nucleons in the *sd* shell.

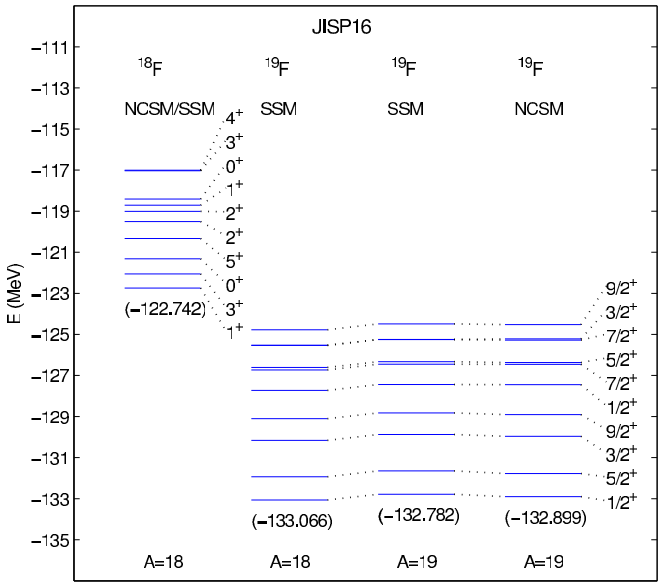

FIG. 3. (Color online) The ground-state energy (in MeV) and low-lying excited-state energies of ^{18}F and ^{19}F obtained by the NCSM and SSM calculations using the effective JISP16 interaction. The tags $A = 18$ and $A = 19$ at the bottom of each column refer to the effective JISP16 interaction obtained with the 2BVC approximation for general A. That is, the tags $A = 18$ and $A = 19$ represent nucleus A used for deriving the primary effective Hamiltonian. In addition, we retain only effective core, one-body, and two-body terms for the secondary effective Hamiltonian.

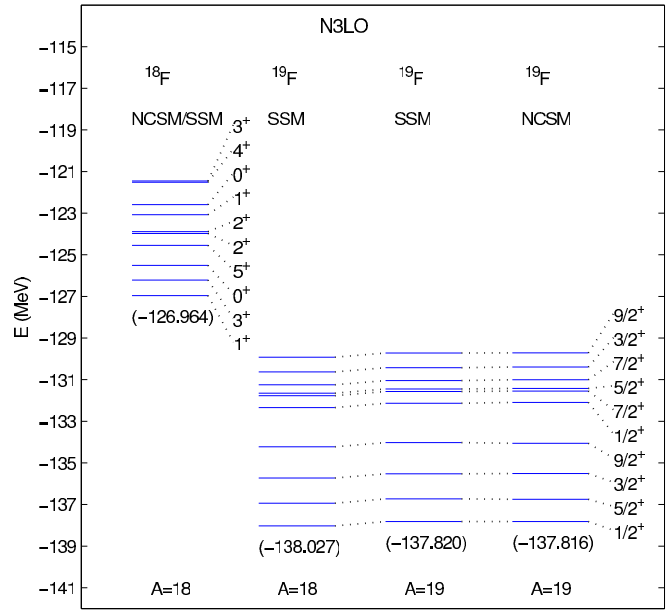

FIG. 4. (Color online) The ground-state energy (in MeV) and low-lying excited-state energies of ^{18}F and ^{19}F obtained by the NCSM and SSM calculations using the effective chiral N3LO interaction. The tags $A = 18$ and $A = 19$ at the bottom of each column refer to the effective JISP16 interaction obtained with the 2BVC approximation for general A. That is, the tags $A = 18$ and $A = 19$ represent nucleus A used for deriving the primary effective Hamiltonian. In addition, we retain only effective core, one-body, and two-body terms for the secondary effective Hamiltonian.

The remaining three columns of Figs. 3 and 4 display two SSM calculations with the secondary effective Hamiltonians and the exact NCSM calculation, all for ^{19}F. The second (third) column shows the results of using the primary effective Hamiltonian for $A = 18$ ($A = 19$) in the 2BVC approximation and solving the resulting SSM for ^{19}F as outlined above. The difference between the second and third columns is interesting since it reflects two different 2BVC approximations. In the second column, we see the effect of ignoring the contributions (both two body and three body) that one additional neutron makes by interacting with all nucleons in ^{18}F. In the third

column we see the effect of ignoring the contributions of all interactions in ^{19}F to the effective three-body valence interaction in ^{19}F. The differences between columns two, three, and four (discussed further below) are almost entirely due to the differences in the ground-state energies; the spectra are nearly the same. The ground-state energies in columns two and three in Figs. 3 and 4 differ over a range from 4 to 211 keV compared with the exact results in column four.

The effects neglected in the two different approximations represented in columns two and three of Figs. 3 and 4 led to small differences in the spectroscopy and, therefore, suggest that both are potentially fruitful paths for further investigation. However, when performing 2BVC calculations for $A > 19$ nuclei (i.e., continuing to retain only core-, one-, and two-body interaction terms) it is natural to expect that the difference between the SSM and NCSM calculations would increase due to the neglect of induced valence three-body, four-body, etc., interactions. The current results suggest that the dominant effect of neglecting these higher-body induced interactions may appear mainly as an overall shift in the spectrum. For the case of ^{19}F, the shift between columns three and four in Fig. 3 (4) shows that the 2BVC approximation for $A = 19$ is responsible for an overall net attraction (repulsion) of about 117 keV (4 keV) which is small on the scale of the overall binding.

The overall shift between columns two and three in Fig. 3 (4) shows that the differences in our derived SSM Hamiltonians produce about a 284 keV (207 keV) displacement in the binding energy. By referring to the results shown in Tables II and III, we find that this displacement in binding energies is attributed approximately to the difference in the core energies (about 80% of the displacement) and to the difference in the sum of single-particle energies for the three valence nucleons (about 20% of the displacement). These displacements may be cast either as diagonal matrix elements of neglected induced 3NFs or as corrections to the core and valence single-particle energies (or to a combination of both). The distribution of these displacements will appear naturally when the 3BVC (i.e., full $a_v = 3$) calculation is performed for ^{19}F.

IV. SUMMARY, CONCLUSIONS, AND OUTLOOK

We calculated A-dependent effective NCSM Hamiltonians, called primary effective Hamiltonians [step 1 that leads to Eq. (10)], in a $4\hbar\Omega$ model space with the realistic JISP16 and chiral N3LO NN interactions. Next, we have solved the NCSM for low-lying eigenstates sufficient to derive a secondary effective Hamiltonian that acts only in the $0\hbar\Omega$ model space for the sd shell yet retains information from the full A-body correlations present in the NCSM solutions [step 2 that leads to Eq. (11)]. We then separate the TBMEs of the secondary effective Hamiltonians into core, one-body, and two-body contributions [steps 3 and 4 that lead to Eq. (12)] which defines to the 2BVC effective Hamiltonian suitable for SSM calculations. Finally, we use these secondary effective Hamiltonians in SSM calculations and compare with exact NCSM results based on the primary Hamiltonians for $A = 18$ and 19.

We estimate that the first OLS transformation on the JISP16 and chiral N3LO NN interactions produces primary effective interactions down to a sufficiently low UV regulator scale that we obtain a nearly common, or universal, primary effective NN interaction. Subsequent processing through the second OLS transformation retains universality features resulting in TBMEs from JISP16 and chiral N3LO that are highly correlated as visualized in Fig. 2.

The SSM spectra for $A = 18$ in the valence space are the same as the low-lying NCSM spectra since our theory of the secondary effective Hamiltonian is derived from the NCSM solutions obtained with the primary effective Hamiltonian. With the 2BVC approximation, for which we present two approaches, there are small differences between the SSM and NCSM spectra for the ^{19}F system. These differences are due to the omitted three-body effective interactions for the ^{19}F system and are observed primarily as overall shifts in the spectra that are mainly due to shifts in the core energies. Close examination of the core, one-body, and two-body components of the secondary effective Hamiltonians shows weak A dependence, which is encouraging for application to heavier nuclei.

We will extend our investigations to obtain more complete results in sd shell by proceeding to a higher $N_{\max}$ model space for NCSM solutions with the primary effective Hamiltonian. We will extend the 2BVC approximation to the 3BVC approximation by including the three-body components of the secondary effective Hamiltonians. In addition, we plan to incorporate initial 3NFs in the NCSM calculations that complement the realistic NN interactions.

ACKNOWLEDGMENTS

This work was supported by Higher Education Council of Turkey (YOK), by The Scientific and Technological Research Council of Turkey (TUBITAK-BIDEB), by the US Department of Energy under Grants No. DESC0008485 (SciDAC/NUCLEI) and No. DE-FG02-87ER40371, by the US National Science Foundation under Grants No. PHYS-0845912 and No. 0904782, by the Ministry of Education and Science of the Russian Federation under Contracts No. P521 and No. 14.V37.21.1297, and by the Russian Foundation of Basic Research within the Project 15-02-06604. Computational resources were provided by the National Energy Research Scientific Computing Center (NERSC), which is supported by the Office of Science of the US Department of Energy under Contract No. DE-AC02-05CH11231.

APPENDIX: TABULATION OF DERIVED TWO-BODY MATRIX ELEMENTS

In this Appendix, we present the tables of our derived 2-body matrix elements (TBMEs).

TABLE IV. The TBMEs (in MeV) of the secondary-*sd*-shell effective Hamiltonian $H_{18}^{P'P}$ obtained from the NCSM calculation with $N_{\max} = 4$, $\hbar\Omega = 14$ MeV, and the JISP16 potential for ^{18}F are shown as well as the TBMEs of its residual valence effective interaction, $V_2^{P'P}$. Pairs of columns are labeled by the A used in Eqs. (1)–(4) to develop the primary effective NCSM Hamiltonian as discussed in the text.

$2j_a$	$2j_b$	$2j_c$	$2j_d$	J	T	$A=18$		$A=19$	
						$H_{18}^{P'P}$	$V_2^{P'P}$	$H_{18}^{P'P}$	$V_2^{P'P}$
1	1	1	1	0	1	−120.176	−2.182	−119.917	−2.181
1	1	3	3	0	1	−0.924	−0.924	−0.924	−0.924
1	1	5	5	0	1	−1.274	−1.274	−1.274	−1.274
3	3	3	3	0	1	−100.477	−0.958	−100.214	−0.958
3	3	5	5	0	1	−3.397	−3.397	−3.396	−3.396
5	5	5	5	0	1	−118.926	−2.525	−118.673	−2.525
1	1	1	1	1	0	−121.296	−3.302	−121.032	−3.296
1	1	1	3	1	0	−0.378	−0.378	−0.383	−0.383
1	1	3	3	1	0	0.231	0.231	0.236	0.236
1	1	3	5	1	0	2.054	2.054	2.052	2.052
1	1	5	5	1	0	−0.936	−0.936	−0.939	−0.939
1	3	1	3	1	0	−112.168	−3.412	−111.902	−3.406
1	3	3	3	1	0	−1.380	−1.380	−1.384	−1.384
1	3	3	5	1	0	1.455	1.455	1.456	1.456
1	3	5	5	1	0	0.525	0.525	0.528	0.528
3	3	3	3	1	0	−100.450	−0.931	−100.181	−0.925
3	3	3	5	1	0	−0.172	−0.172	−0.173	−0.173
3	3	5	5	1	0	2.511	2.511	2.508	2.508
3	5	3	5	1	0	−113.957	−5.997	−113.698	−5.996
3	5	5	5	1	0	3.579	3.579	3.580	3.580
5	5	5	5	1	0	−117.448	−1.047	−117.191	−1.043
1	3	1	3	1	1	−108.749	0.007	−108.487	0.009
1	3	3	5	1	1	0.042	0.042	0.042	0.042
3	5	3	5	1	1	−108.057	−0.097	−107.798	−0.096
1	3	1	3	2	0	−110.023	−1.267	−109.760	−1.264
1	3	1	5	2	0	−2.969	−2.969	−2.968	−2.968
1	3	3	5	2	0	−1.873	−1.873	−1.873	−1.873
1	5	1	5	2	0	−117.279	−0.081	−117.021	−0.079
1	5	3	5	2	0	−1.597	−1.597	−1.597	−1.597
3	5	3	5	2	0	−112.093	−4.133	−111.826	−4.124
1	3	1	3	2	1	−109.374	−0.618	−109.113	−0.617
1	3	1	5	2	1	1.504	1.504	1.504	1.504
1	3	3	3	2	1	0.185	0.185	0.185	0.185
1	3	3	5	2	1	0.601	0.601	0.601	0.601
1	3	5	5	2	1	1.005	1.005	1.005	1.005
1	5	1	5	2	1	−118.667	−1.469	−118.411	−1.469
1	5	3	3	2	1	−0.840	−0.840	−0.840	−0.840
1	5	3	5	2	1	−0.374	−0.374	−0.374	−0.374
1	5	5	5	2	1	−0.780	−0.780	−0.780	−0.780
3	3	3	3	2	1	−99.766	−0.247	−99.503	−0.247
3	3	3	5	2	1	−0.933	−0.933	−0.933	−0.933
3	3	5	5	2	1	−0.730	−0.730	−0.730	−0.730
3	5	3	5	2	1	−108.232	−0.272	−107.973	−0.271
3	5	5	5	2	1	−0.352	−0.352	−0.352	−0.352
5	5	5	5	2	1	−117.617	−1.216	−117.364	−1.216
1	5	1	5	3	0	−121.030	−3.832	−120.770	−3.828
1	5	3	3	3	0	0.068	0.068	0.066	0.066
1	5	3	5	3	0	1.373	1.373	1.375	1.375
1	5	5	5	3	0	−1.766	−1.766	−1.768	−1.768
3	3	3	3	3	0	−102.271	−2.752	−102.006	−2.750
3	3	3	5	3	0	2.000	2.000	1.998	1.998
3	3	5	5	3	0	0.961	0.961	0.963	0.963
3	5	3	5	3	0	−108.629	−0.669	−108.367	−0.665
3	5	5	5	3	0	2.308	2.308	2.306	2.306
5	5	5	5	3	0	−117.125	−0.724	−116.870	−0.722
1	5	1	5	3	1	−117.022	0.176	−116.765	0.177
1	5	3	5	3	1	−0.356	−0.356	−0.356	−0.356
3	5	3	5	3	1	−107.888	0.072	−107.629	0.073
3	5	3	5	4	0	−112.314	−4.354	−112.049	−4.347
3	5	3	5	4	1	−109.863	−1.903	−109.605	−1.903
3	5	5	5	4	1	−1.303	−1.303	−1.303	−1.303
5	5	5	5	4	1	−116.766	−0.365	−116.513	−0.365
5	5	5	5	5	0	−120.329	−3.928	−120.075	−3.927

TABLE V. The TBMEs (in MeV) of the secondary *sd*-shell effective Hamiltonian $H_{18}^{P'P}$ obtained from the NCSM calculation with $N_{\max} = 4$, $\hbar\Omega = 14$ MeV, and chiral N3LO potential for ^{18}F are shown as well as the TBMEs of its residual valence effective interaction, $V_2^{P'P}$. Pairs of columns are labeled by the A used in Eqs. (1)–(4) to develop the primary effective NCSM Hamiltonian as discussed in the text.

$2j_a$	$2j_b$	$2j_c$	$2j_d$	J	T	$A=18$		$A=19$	
						$H_{18}^{P'P}$	$V_2^{P'P}$	$H_{18}^{P'P}$	$V_2^{P'P}$
1	1	1	1	0	1	−124.196	−2.106	−123.978	−2.104
1	1	3	3	0	1	−0.991	−0.991	−0.991	−0.991
1	1	5	5	0	1	−1.268	−1.268	−1.268	−1.268
3	3	3	3	0	1	−108.265	−0.858	−108.086	−0.857
3	3	5	5	0	1	−3.538	−3.538	−3.537	−3.537
5	5	5	5	0	1	−123.099	−2.278	−122.914	−2.277
1	1	1	1	1	0	−125.152	−3.089	−124.960	−3.086
1	1	1	3	1	0	−0.022	−0.022	−0.023	−0.023
1	1	3	3	1	0	−0.175	−0.175	−0.175	−0.175
1	1	3	5	1	0	2.315	2.315	2.314	2.314
1	1	5	5	1	0	−0.750	−0.750	−0.750	−0.750
1	3	1	3	1	0	−118.632	−3.870	−118.418	−3.866
1	3	3	3	1	0	−1.149	−1.149	−1.148	−1.148
1	3	3	5	1	0	1.568	1.568	1.568	1.568
1	3	5	5	1	0	0.355	0.355	0.355	0.355
3	3	3	3	1	0	−108.280	−0.873	−108.101	−0.872
3	3	3	5	1	0	−0.217	−0.217	−0.217	−0.217
3	3	5	5	1	0	2.265	2.265	2.264	2.264
3	5	3	5	1	0	−119.761	−5.620	−119.549	−5.616
3	5	5	5	1	0	3.377	3.377	3.375	3.375
5	5	5	5	1	0	−121.832	−1.011	−121.646	−1.009
1	3	1	3	1	1	−114.838	−0.076	−114.627	−0.075
1	3	3	5	1	1	−0.157	−0.157	−0.156	−0.156
3	5	3	5	1	1	−114.478	−0.337	−114.268	−0.335
1	3	1	3	2	0	−116.128	−1.576	−116.126	−1.574
1	3	1	5	2	0	−2.623	−2.623	−2.622	−2.622
1	3	3	5	2	0	−1.980	−1.980	−1.978	−1.978
1	5	1	5	2	0	−121.972	−0.503	−121.757	−0.501
1	5	3	5	2	0	−1.703	−1.703	−1.702	−1.702

TABLE V. (*Continued.*)

$2j_a$	$2j_b$	$2j_c$	$2j_d$	J	T	$A=18$		$A=19$	
						$H_{18}^{P'P}$	$V_2^{P'P}$	$H_{18}^{P'P}$	$V_2^{P'P}$
3	5	3	5	2	0	−118.482	−4.341	−118.271	−4.338
1	3	1	3	2	1	−115.422	−0.660	−115.211	−0.659
1	3	1	5	2	1	1.569	1.569	1.569	1.569
1	3	3	3	2	1	0.188	0.188	0.188	0.188
1	3	3	5	2	1	0.695	0.695	0.695	0.695
1	3	5	5	2	1	0.883	0.883	0.883	0.883
1	5	1	5	2	1	−122.903	−1.434	−122.688	−1.432
1	5	3	3	2	1	−0.869	−0.869	−0.869	−0.869
1	5	3	5	2	1	−0.298	−0.298	−0.298	−0.298
1	5	5	5	2	1	−0.802	−0.802	−0.802	−0.802
3	3	3	3	2	1	−107.666	−0.259	−107.487	−0.258
3	3	3	5	2	1	−0.885	−0.885	−0.885	−0.885
3	3	5	5	2	1	−0.813	−0.813	−0.813	−0.813
3	5	3	5	2	1	−114.549	−0.408	−114.340	−0.407
3	5	5	5	2	1	−0.359	−0.359	−0.359	−0.359
5	5	5	5	2	1	−122.077	−1.256	−121.892	−1.255
1	5	1	5	3	0	−125.266	−3.797	−125.049	−3.793

TABLE V. (*Continued.*)

$2j_a$	$2j_b$	$2j_c$	$2j_d$	J	T	$A=18$		$A=19$	
						$H_{18}^{P'P}$	$V_2^{P'P}$	$H_{18}^{P'P}$	$V_2^{P'P}$
1	5	3	3	3	0	0.155	0.155	0.154	0.154
1	5	3	5	3	0	1.206	1.206	1.205	1.205
1	5	5	5	3	0	−1.648	−1.648	−1.647	−1.647
3	3	3	3	3	0	−110.003	−2.596	−109.822	−2.593
3	3	3	5	3	0	1.819	1.819	1.818	1.818
3	3	5	5	3	0	0.564	0.564	0.563	0.563
3	5	3	5	3	0	−115.233	−1.092	−115.023	−1.090
3	5	5	5	3	0	1.940	1.940	1.939	1.939
5	5	5	5	3	0	−121.768	−0.947	−121.583	−0.946
1	5	1	5	3	1	−121.476	−0.007	−121.262	−0.006
1	5	3	5	3	1	−0.094	−0.094	−0.094	−0.094
3	5	3	5	3	1	−114.287	−0.146	−114.078	−0.145
3	5	3	5	4	0	−118.684	−4.543	−118.472	−4.539
3	5	3	5	4	1	−116.134	−1.993	−115.924	−1.991
3	5	5	5	4	1	−1.319	−1.319	−1.318	−1.318
5	5	5	5	4	1	−121.190	−0.369	−121.006	−0.369
5	5	5	5	5	0	−124.545	−3.724	−124.358	−3.721

[1] I. Stetcu, B. R. Barrett, P. Navrátil, and J. P. Vary, Phys. Rev. C **71**, 044325 (2005).

[2] P. Navrátil, W. E. Ormand, C. Forssen, and E. Caurier, Eur. Phys. J. A **25**, 481 (2005).

[3] I. Stetcu, B. R. Barrett, P. Navrátil, and J. P. Vary, Phys. Rev. C **73**, 037307 (2006).

[4] A. Nogga, P. Navrátil, B. R. Barrett, and J. P. Vary, Phys. Rev. C **73**, 064002 (2006).

[5] R. Roth and P. Navrátil, Phys. Rev. Lett. **99**, 092501 (2007).

[6] P. Maris, J. P. Vary, and A. M. Shirokov, Phys. Rev. C **79**, 014308 (2009).

[7] P. Maris, A. M. Shirokov, and J. P. Vary, Phys. Rev. C **81**, 021301(R) (2010).

[8] P. Maris, J. P. Vary, P. Navrátil, W. E. Ormand, H. Nam, and D. J. Dean, Phys. Rev. Lett. **106**, 202502 (2011).

[9] C. Cockrell, J. P. Vary, and P. Maris, Phys. Rev. C **86**, 034325 (2012).

[10] P. Maris and J. P. Vary, Int. J. Mod. Phys. E **22**, 1330016 (2013).

[11] P. Navrátil, M. Thoresen, and B. R. Barrett, Phys. Rev. C **55**, R573 (1997).

[12] P. Navrátil, J. P. Vary, and B. R. Barrett, Phys. Rev. Lett. **84**, 5728 (2000).

[13] P. Navrátil, J. P. Vary, and B. R. Barrett, Phys. Rev. C **62**, 054311 (2000).

[14] P. Navrátil, J. P. Vary, W. E. Ormand, and B. R. Barrett, Phys. Rev. Lett. **87**, 172502 (2001).

[15] P. Navrátil, V. G. Gueorguiev, J. P. Vary, W. E. Ormand, and A. Nogga, Phys. Rev. Lett. **99**, 042501 (2007).

[16] B. R. Barrett, P. Navrátil, and J. P. Vary, Prog. Part. Nucl. Phys. **69**, 131 (2013).

[17] E. D. Jurgenson, P. Maris, R. J. Furnstahl, P. Navrátil, W. E. Ormand, and J. P. Vary, Phys. Rev. C **87**, 054312 (2013).

[18] A. M. Shirokov, V. A. Kulikov, P. Maris, and J. P. Vary, in *NN and 3N Interactions*, edited by L. D. Blokhintsev and I. I. Strakovsky (Nova Science, Hauppauge, NY, 2014), Chap. 8, p. 231, http://www.novapublishers.com/catalog/product_info.php?products_id=49997.

[19] P. Maris, J. P. Vary, A. Calci, J. Langhammer, S. Binder, and R. Roth, Phys. Rev. C **90**, 014314 (2014).

[20] S. Fujii, T. Mizusaki, T. Otsuka, T. Sebe, and A. Arima, Phys. Lett. B **650**, 9 (2007).

[21] A. F. Lisetskiy, B. R. Barrett, M. K. G. Kruse, P. Navrátil, I. Stetcu, and J. P. Vary, Phys. Rev. C **78**, 044302 (2008).

[22] S. K. Bogner, H. Hergert, J. D. Holt, A. Schwenk, S. Binder, A. Calci, J. Langhammer, and R. Roth, Phys. Rev. Lett. **113**, 142501 (2014).

[23] G. R. Jansen, J. Engel, G. Hagen, P. Navrátil, and A. Signoracci, Phys. Rev. Lett. **113**, 142502 (2014).

[24] S. Okubo, Prog. Theor. Phys. **12**, 603 (1954).

[25] K. Suzuki and S. Y. Lee, Prog. Theor. Phys. **64**, 2091 (1980).

[26] K. Suzuki, Prog. Theor. Phys. **68**, 246 (1982); K. Suzuki and R. Okamoto, *ibid.* **70**, 439 (1983).

[27] A. M. Shirokov, J. P. Vary, A. I. Mazur, and T. A. Weber, Phys. Lett. B **644**, 33 (2007); A Fortran code for JISP16 is available at nuclear.physics.iastate.edu

[28] D. R. Entem and R. Machleidt, Phys. Rev. C **68**, 041001 (2003).

[29] C. P. Viazminsky and J. P. Vary, J. Math. Phys. **42**, 2055 (2001).

[30] A. F. Lisetskiy, M. K. G. Kruse, B. R. Barrett, P. Navrátil, I. Stetcu, and J. P. Vary, Phys. Rev. C **80**, 024315 (2009).

[31] P. Sternberg, E. G. Ng, C. Yang, P. Maris, J. P. Vary, M. Sosonkina, and H. V. Le, *Procedia of the 2008 ACM/IEEE Conference on Supercomputing (SC 2008)* (IEEE Press, Piscataway, NJ, 2008), pp. 15:1–12.

[32] P. Maris, M. Sosonkina, J. P. Vary, E. G. Ng, and C. Yang, *Procedia Computer Science 1 (May 2010, ICCS 2010)* (Elsevier, Amsterdam, 2010), pp. 97–106.

[33] H. M. Aktulga, C. Yang, E. G. Ng, P. Maris, and J. P. Vary, *Lecture Notes in Computer Science 7484 (2012)* (Springer, Heidelberg, 2012), pp. 830–842.
[34] E. Caurier and F. Nowacki, Acta Phys. Pol. B **30**, 705 (1999).
[35] E. Caurier, G. Martinez-Pinedo, F. Nowacki, A. Poves, J. Retamosa, and A. P. Zuker, Phys. Rev. C **59**, 2033 (1999).
[36] E. Caurier, P. Navrátil, W. E. Ormand, and J. P. Vary, Phys. Rev. C **64**, 051301(R) (2001).
[37] J. P. Vary and S. N. Yang, Phys. Rev. C **15**, 1545 (1977), and references therein.
[38] S. A. Coon, M. I. Avetian, M. K. G. Kruse, U. van Kolck, P. Maris, and J. P. Vary, Phys. Rev. C **86**, 054002 (2012).
[39] S. N. More, A. Ekström, R. J. Furnstahl, G. Hagen, and T. Papenbrock, Phys. Rev. C **87**, 044326 (2013).